Tests of mode coupling theory in a simple model for two-component miscible polymer blends

2007 J. Phys.: Condens. Matter 19 466112

(http://iopscience.iop.org/0953-8984/19/46/466112)

IOP PUBLISHING JOURNAL OF PHYSICS: CONDENSED MATTER

J. Phys.: Condens. Matter **19** (2007) 466112 (18pp) doi:10.1088/0953-8984/19/46/466112

Tests of mode coupling theory in a simple model for two-component miscible polymer blends

A J Moreno[1,4] **and J Colmenero**[1,2,3]

[1] Centro de Física de Materiales (CSIC-UPV/EHU), Apartado 1072, 20080 San Sebastián, Spain
[2] Departamento de Física de Materiales, Universidad del País Vasco (UPV/EHU), Apartado 1072, 20080 San Sebastián, Spain
[3] Donostia International Physics Center, Paseo Manuel de Lardizabal 4, 20018 San Sebastián, Spain

E-mail: wabmosea@ehu.es

Received 6 August 2007, in final form 26 September 2007
Published 26 October 2007
Online at stacks.iop.org/JPhysCM/19/466112

Abstract

We present molecular dynamics simulations of the structural relaxation of a simple bead–spring model for polymer blends. The introduction of a different monomer size induces a large timescale separation for the dynamics of the two components. Simulation results for a large set of observables probing density correlations, Rouse modes, and orientations of bond and chain end-to-end vectors are analysed within the framework of the mode coupling theory (MCT). An unusually large value of the exponent parameter is obtained. This feature suggests the possibility of an underlying higher-order MCT scenario for dynamic arrest.

(Some figures in this article are in colour only in the electronic version)

1. Introduction

Polymer blends are soft-matter systems which exhibit 'dynamic asymmetry', meaning that, starting from two homopolymers with different mobilities, two separated segmental dynamics can still be observed in the blend. Phenomenological approaches usually consider thermally driven concentration fluctuations [1] and self-concentration effects induced by chain connectivity [2] as key ingredients for structural relaxation in polymer blends [3]. A recent approach combines self-concentration effects with ideas of the Adam–Gibbs theory [4]. For most of the investigated systems, dynamics of the two components in the blend display qualitatively similar features. However, recent experimental results from nuclear magnetic resonance (NMR) [5, 6], dielectric spectroscopy [7–11], or neutron scattering [12, 13] suggest that a rather different scenario arises when the two homopolymers exhibit very different glass transition temperatures. Hence, for dilute concentrations of the fast component, the

[4] Author to whom any correspondence should be addressed.

two components in the blend exhibit strong dynamic immiscibility. A large separation in their relaxation times is observed, which can even be of 12 orders of magnitude in blends of poly(ethylene oxide)/poly(methyl methacrylate) (PEO/PMMA) for an extreme dilution of PEO [6]. In such conditions the motion of the chains of the fast component takes place in a slowly relaxing matrix formed by the slow component, providing a connection with the problem of confinement in host media with interconnected voids.

We have recently performed an investigation on the structural relaxation dynamics of a simple bead–spring model for polymer blends [14]. The introduction of monomer size disparity between the two components induces a large timescale separation for low concentrations of the fast component, which displays unusual relaxation features. Hence, density–density correlators exhibit logarithmic decays over time intervals of even four decades and a concave-to-convex crossover by varying the thermodynamic state point (i.e. the control parameters) or the wavevector [14]. Dynamic features observed for this simplified model are supported by recent fully atomistic simulations for the PEO/PMMA blend [12].

We have discussed the unusual features reported in [14] within the framework of the mode coupling theory (MCT) of the glass transition [15, 16], and suggested an underlying higher-order MCT transition as the origin of the observed anomalous relaxation scenario. Higher-order MCT transitions were initially predicted by schematic models [17], and later derived for simplified models of short-range attractive colloids [18, 19]. These systems show two different mechanisms for dynamic arrest: steric repulsion characteristic of colloidal systems, and formation of reversible bonds, induced by the short-range attraction. Coexistence of both mechanisms of very different localization lengths [18, 19] yields a higher-order MCT transition in a certain region of the temperature–density plane. The mentioned anomalous relaxation features are derived from the MCT equations as specific solutions associated with the higher-order point [18–21].

Results for the mean squared displacements and density–density correlators in the bead–spring polymer blend of [14] display striking similarities with qualitative features associated with higher-order MCT transitions. Similar results have also been observed in later simulations of binary mixtures of non-bonded particles with large size disparity, both for soft [22, 23] and ultrasoft interactions [24]. Finally, very recent two-dimensional NMR experiments on a polymer–plasticizer system have revealed logarithmic relaxation for a strongly confined plasticizer [25]. Hence, this collection of similar experimental and simulation results suggest a common relaxation scenario for multicomponent systems exhibiting strong dynamic asymmetry. Moreover, the mentioned analogies with short-range attractive colloids suggest that the higher-order MCT scenario might be a general feature of systems showing several mechanisms for dynamic arrest. For the mentioned polymeric and non-polymeric mixtures, we have suggested bulk-like caging and confinement [14, 22, 23]. These mechanisms would be respectively induced by the presence of neighbouring small particles and by the slow matrix formed by the large particles.

It is worth mentioning that solutions of the MCT equations for a fluid of hard spheres confined in a disordered matrix of *strictly static* obstacles explicitly reveal the existence of a higher-order transition [26]. As discussed in [26], the strictly static nature of the matrix induces differences from the former mixtures, where the matrix shows a slow relaxation. Hence, though they share common features for the dynamics of the confined component, a comparison of results between both kind of mixtures must be made with care.

The test of MCT predictions for the bead–spring blend model reported in [14] was restricted to density–density correlators. In this paper we present a systematic test for a large set of correlators probing different dynamic features as Rouse modes or orientations of bond and chain end-to-end vectors. Consistent with MCT predictions, a common set of dynamic

exponents provides a good description of dynamic correlators in the early-middle stage of the structural α-relaxation. Consistent with previous results [14], the unusually large value obtained for the exponent parameter suggests that the observed anomalous relaxation features might be associated with an underlying higher-order MCT scenario.

This paper is organized as follows. In section 2 we summarize the main details of the simulated model. In section 3 we present simulation results for static correlations. The main predictions of MCT are exposed in section 4. We discuss within the framework of MCT relaxation features of the slow and fast component in, respectively, sections 5 and 6. Conclusions are given in section 7.

2. Model and simulation details

The model introduces a binary mixture of bead–spring chains (of the species A and B). Each chain consists of $N = 10$ monomers of mass $m = 1$. All the monomers in the same chain belong to the same species (i.e. all them are A-like or B-like). Two given monomers (placed in the same chain or different ones) interact through a soft-sphere potential plus a quadratic term, $V_{\alpha\beta}(r) = 4\epsilon[(\sigma_{\alpha\beta}/r)^{12} - C_0 + C_2(r/\sigma_{\alpha\beta})^2]$, where $\epsilon = 1$ and $\alpha, \beta \in \{A, B\}$. The interaction is zero beyond a cutoff distance $r_c = c\sigma_{\alpha\beta}$, with $c = 1.15$. Continuity of potential and forces at $r = r_c$ is guaranteed by setting the values $C_0 = 7c^{-12}$ and $C_2 = 6c^{-14}$. The radii of the different pair interactions are $\sigma_{BB} = 1$, $\sigma_{AA} = 1.6\sigma_{BB}$, and $\sigma_{AB} = 1.3\sigma_{BB}$. Chain connectivity is introduced by a FENE bonding potential [27], $V_{\alpha\alpha}^{FENE}(r) = -kR_0^2\epsilon \ln[1 - (R_0\sigma_{\alpha\alpha})^{-2}r^2]$, between consecutive monomers, with $k = 15$ and $R_0 = 1.5$. The superposition of $V_{\alpha\beta}(r)$ and $V_{\alpha\alpha}^{FENE}(r)$ provides an effective bonding potential for connected monomers with a sharp minimum at $r = 0.985\sigma_{\alpha\beta}$, which makes bond crossing impossible.

The blend composition is defined as $x_B = N_B/(N_A + N_B)$, where N_α is the number of α-chains. All the data presented here correspond to a fixed composition $x_B = 0.3$ (we have simulated a mixture of $N_A = 210$ and $N_B = 90$ chains). We use a packing fraction $\phi = (\pi/6)L^{-3}[N_A\sigma_{AA}^3 + N_B\sigma_{BB}^3] = 0.53$, with L the side of the cubic simulation cell. The value $\phi = 0.53$ is comparable to those used in simulations of slow relaxation in simple liquids [28, 29]. In the following, temperature T, distance, wavevector q, and time t will be given, respectively, in units of ϵ/k_B, σ_{BB}, σ_{BB}^{-1}, and $\sigma_{BB}(m/\epsilon)^{1/2}$.

The system is prepared by placing the chains randomly in the simulation cell, with a constraint that avoids overlapping of monomer cores. The Newtonian equations of motion are integrated in the velocity Verlet scheme [30], with a time step ranging from 2×10^{-4} to 5×10^{-3} for, respectively, the highest and the lowest investigated T. Standard periodic boundary conditions are used for calculation of monomer–monomer distances entering in the interactions. Computational expense for the latter calculation is reduced by implementing a standard link-cell method [30]. The system is thermalized at the selected temperature by periodic velocity rescaling. Then the equilibrium run for data acquisition is performed in the microcanonical ensemble (constant energy). During this run no drift in thermodynamic quantities is observed nor ageing effects in dynamic correlators computed for different time origins. Statistical averages at a given state point are typically performed over 20–40 independent runs.

3. Static properties

In this section we provide information about static correlations in the bead–spring blend. We compute normalized partial static structure factors $S_{\alpha\beta}(q) = \langle\rho_\alpha(q,0)\rho_\beta^*(q,0)\rangle/(N\sqrt{N_\alpha N_\beta})$. The quantity $\rho_\alpha(q,t)$ is the density fluctuation for wavevector q and is defined as $\rho_\alpha(q,t) = \sum_j \exp[i\mathbf{q}\cdot\mathbf{r}_j^\alpha(t)]$, the sum extending over all the particles of the species $\alpha \in$ {A,B}. Figure 1

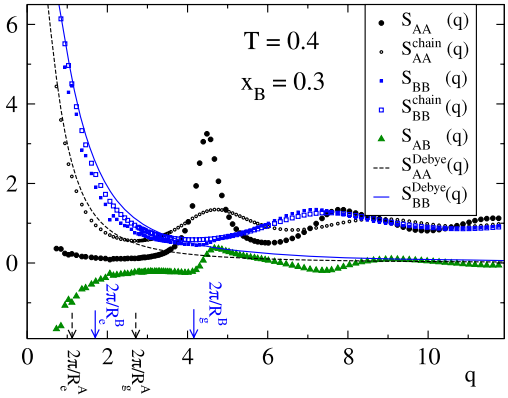

Figure 1. Partial static structure factors, $S_{AA}(q)$, $S_{BB}(q)$ and $S_{AB}(q)$, at $T = 0.4$. Also included are the chain form factors, $S_{AA}^{chain}(q)$, $S_{BB}^{chain}(q)$, as well as the corresponding Debye functions, $S_{AA}^{Debye}(q)$, $S_{BB}^{Debye}(q)$. Arrows indicate the wavevectors $q = 2\pi/R_{e,g}^{\alpha}$, where R_e^{α} and R_g^{α} are, respectively, the chain end-to-end distance and gyration radius of the species α.

shows, for a low temperature $T = 0.4$, results for A–A, B–B, and A–B pairs. Intrachain static structure factors (i.e. chain form factors), $S_{\alpha\alpha}^{chain}(q)$, are also displayed. The latter quantities are computed by restricting the product $\rho_\alpha(q,0)\rho_\alpha^*(q,0) = \sum_{j,k} \exp\{i\mathbf{q}\cdot[\mathbf{r}_j^\alpha(0) - \mathbf{r}_k^\alpha(0)]\}$ over pairs of monomers j, k belonging to the same chain. A sharp maximum is observed in $S_{AA}(q)$ at $q = 4.5$, which corresponds to a typical distance of 1.4 between A-monomers. Results for $S_{AA}(q)$ are qualitatively similar to those reported for the *homopolymer* case in a similar bead–spring model [29, 31]. A weak low-q structure is observed in the present case, which originates from the presence of 'holes' in the matrix of A-monomers. These holes are created by the inclusion of the B-monomers. The negative values of $S_{AB}(q)$ observed at small wavevectors are a signature of anticorrelation effects between A- and B-monomers at large distances, and indicate a moderate degree of demixing. This feature is illustrated in figure 2, which shows a typical configuration of the B-chains. The latter are not homogeneously distributed but form a sort of cluster structure.

The partial static structure factor for B–B pairs, $S_{BB}(q)$, exhibits a rather different q-dependence (figure 1). From a comparison with the form factor for B-chains, $S_{BB}^{chain}(q)$, it is clear that $S_{BB}(q)$ is largely dominated by intrachain contributions, as expected for high dilution of the B-chains in the matrix formed by the A-chains. The peak at $q = 7.2$ corresponds to a typical distance of 0.87 between B-monomers.

Data for the chain form factors in figure 1 are also compared with the Debye function [32, 33], $S_{\alpha\alpha}^{Debye}(q) = 2Nq^{-4}(R_g^\alpha)^{-4}\{\exp[-q^2(R_g^\alpha)^2] + q^2(R_g^\alpha)^2 - 1\}$, which is obtained by assuming a Gaussian distribution of monomer–monomer distances within the chain [32, 33]. As previously observed for the homopolymer case [31], Gaussian statistics approximately work at low q but clearly break down for wavevectors probing distances smaller than the chain gyration radius R_g^α. The magnitude of the deviations of simulation data from the Debye function is similar to observations for the homopolymer case [31]. Hence, chain statistics is not significantly affected by blending.

4. Main predictions of MCT

In this section we summarize some of the main predictions of the MCT for the glass transition. Extensive reviews can be found, for example in [15, 16, 34–36]. In its ideal version, MCT

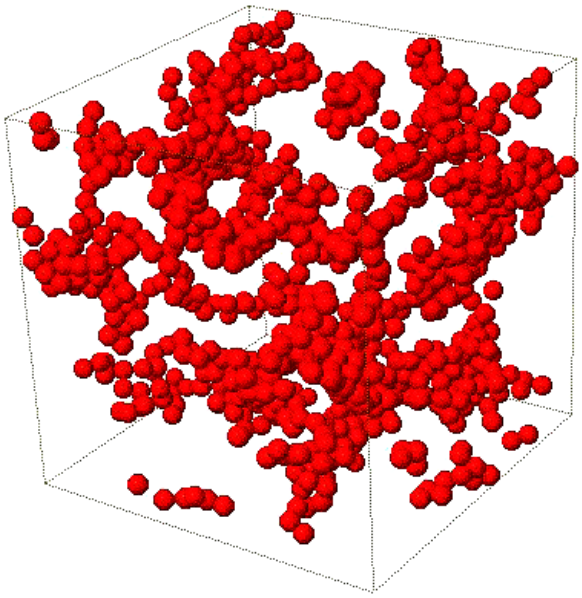

Figure 2. A typical configuration of the B-chains.

predicts a sharp transition from an ergodic liquid to a non-ergodic glassy state for a given value of the relevant control parameter ξ (in the following the temperature, T, though results given below are valid for any ξ). On approaching the transition point $T = T_c$, MCT establishes a set of quantitative predictions for any correlator coupled to density fluctuations, $\Phi(t)$. An example is normalized density–density correlators of wavevector q, $F_{\alpha\alpha}(q,t) = \langle \rho_\alpha(q,t)\rho^*_\alpha(q,0)\rangle / S_{\alpha\alpha}(q)$, for the species α. At the critical temperature $T = T_c$ the long-time limit of $\Phi(t)$ jumps from zero to a non-zero value, denoted as the *critical* non-ergodicity parameter, Φ^c. In the standard case (*type-B* transitions) the jump in $\Phi(t)$ is discontinuous, i.e. Φ^c takes a finite positive value.

For ergodic states close to the transition point Φ usually exhibits a first decay to a plateau, whose time extension increases as the transition is approached. This plateau regime corresponds to the temporary trapping of each particle within the cage formed by its neighbouring ones, i.e. the well-known caging effect which is generally present in supercooled liquids or jammed systems, for example. At times longer than the so-called first MCT timescale t_σ, the correlator Φ starts a second decay from the plateau to zero. This second decay is commonly known as the α-process and represents the full decorrelation of the system from its initial configuration, i.e. the structural relaxation. According to MCT, the initial part of the α-process (denoted as the von Schweidler regime) is given by a power-law decay $\propto -t^b$, with $0 \leqslant b \leqslant 1$. A power-law series expansion extends the description of the α-decay to longer times:

$$\Phi(t) = \Phi^c - h_\Phi (t/\tau_\alpha)^b + h^{(2)}_\Phi (t/\tau_\alpha)^{2b} + \mathrm{O}(t^{3b}). \tag{1}$$

The prefactors h_Φ and $h^{(2)}_\Phi$ are state point-independent and are different for each correlator Φ. On the contrary, the von Schweidler exponent b is common to all correlators. The characteristic timescale of the α-relaxation, τ_α, is the second MCT timescale. It is also unique for all correlators, and diverges at the transition point as $\propto (T - T_c)^{-\gamma}$ (see below). The α-decay can often be described by an empirical Kohlrausch–Williams–Watt (KWW) function,

$\propto \exp[-(t/\tau)^{\beta_\Phi}]$, with a Φ-dependent stretching exponent $0 < \beta_\Phi < 1$. An interesting prediction of MCT [37] is that $\beta_q = b$ and $\tau \propto q^{-1/b}$ in the limit of large q, both for density–density [$F(q,t)$], and self-correlators, $F_\alpha^s(q,t) = \langle \sum_j \exp\{i\mathbf{q}\cdot[\mathbf{r}_{\alpha,j}(t) - \mathbf{r}_{\alpha,j}(0)]\}\rangle/(NN_\alpha)$. This result [23, 28, 29, 31, 38–41] provides a consistency test for data analysis.

Another prediction of MCT for state points close to the transition point is the power-law dependence of the diffusivity and the relaxation time τ_x^Φ:

$$\tau_x^\Phi, D^{-1} \propto (T - T_c)^{-\gamma}. \tag{2}$$

The relaxation time τ_x^Φ of the correlator Φ is defined as the time where $\Phi(t)$ decays to some small value x, provided it is well below the plateau. The time–temperature superposition principle of the MCT establishes that, for t much longer than the first timescale t_σ, $\Phi(t/\tau_\alpha) = \tilde{\Phi}$, where $\tilde{\Phi}$ is a Φ-dependent scaling function. According to this prediction, for a fixed x the ratio τ_x^Φ/τ_α is temperature-independent for any $\tau_x^\Phi \gg t_\sigma$, i.e. $\tau_x^\Phi \propto \tau_\alpha$. In other words, τ_x^Φ will be Φ-modulated but will follow the same power-law behaviour in T as the α-relaxation time τ_α (*even if* $\tau_x^\Phi \gg \tau_\alpha$). Note that, in the MCT terminology, τ_α is a single timescale, though its value can be approximately probed by evaluating dynamic correlators Φ for which $\tau_x^\Phi \sim \tau_\alpha$. This is the case of, for example, the density–density correlator $F(q,t)$ for wavevector q at the maximum of the static structure factor $S(q)$, since the former probes decorrelation over typical distances between nearest-neighbour particles. The relaxation time of $F(q,t)$ is indeed often denoted as the 'α-relaxation time', though in the context of MCT the latter strictly corresponds to τ_α.

The exponent γ in equation (2) is given by the relation

$$\gamma = \frac{1}{2a} + \frac{1}{2b}, \tag{3}$$

with $0 \leqslant a \leqslant 0.395$. Hence $\gamma \geqslant 1.766$. The critical exponents a, b, and γ are unequivocally related to the so-called exponent parameter λ through

$$\lambda = \frac{\Gamma^2(1+b)}{\Gamma(1+2b)} = \frac{\Gamma^2(1-a)}{\Gamma(1-2a)}, \tag{4}$$

where Γ is the Gamma function. The exponent parameter λ is unequivocally determined by the static correlations (i.e. by the total and partial static structure factors) at the transition point $T = T_c$. For type-B transitions it takes values $1/2 \leqslant \lambda \leqslant 1$.

When numerical solutions of the MCT equations are not available the non-ergodicity parameters, prefactors and exponents in equations (1)–(4)—which are system-dependent quantities controlled by static correlations—are empirically obtained as fit parameters from simulation or experimental data. Consistency of the data analysis requires that the set of exponents so obtained fulfils both equations (3) and (4).

5. Dynamics of the slow component in the blend

Figure 3 shows results for the mean squared displacement averaged over all the monomers, $\langle \Delta r_\alpha^2(t)\rangle$, for both A- and B-chains. The introduction of monomer size disparity, $\sigma_{AA}/\sigma_{BB} = 1.6$, induces a large timescale separation between the two components, for low concentration of the B-chains, by decreasing temperature. Now we analyse relaxation features for the slow A-component. Results for the fast B-component are analysed in the next section.

Figures 4–8 show, for the A-chains, a consistent test, i.e. with a common set of exponents, of MCT predictions for several dynamic correlators, diffusivities, and relaxation times. Figure 4 shows, for several wavevectors, results at $T = 0.4$ for the intrachain coherent correlator $F_{AA}^{chain}(q,t)$. The latter is computed as $\langle \sum_{j,k} \exp\{i\mathbf{q}\cdot[\mathbf{r}_{\alpha,j}(t) - \mathbf{r}_{\alpha,k}(0)]\}\rangle/[NN_\alpha S_{\alpha\alpha}^{chain}(q)]$,

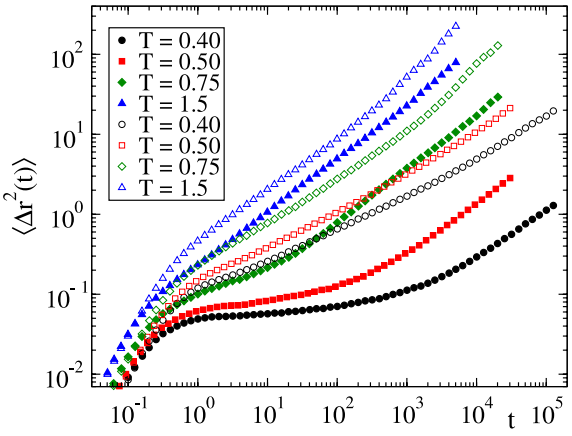

Figure 3. Mean squared displacement at different temperatures for both components. Filled and empty symbols correspond, respectively, to A- and B-chains.

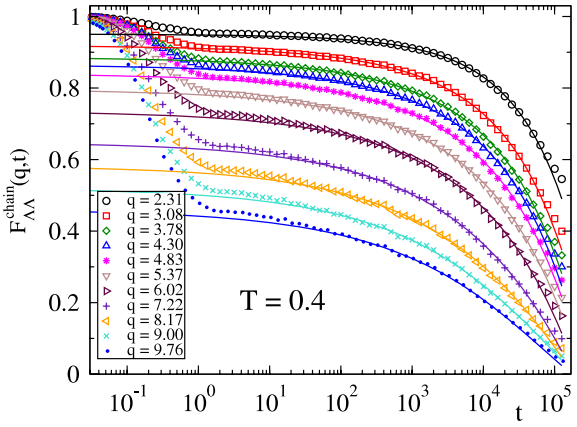

Figure 4. Symbols: for different wavevectors, intrachain coherent correlator for A–A pairs, $F_{AA}^{chain}(q,t)$, at $T = 0.4$. Lines are fits to equation (1) with an exponent $b = 0.30$.

for any species α. In this equation the sum only includes j, k pairs belonging to the same α-chain. Figure 5 shows normalized correlators of the Rouse modes $\phi_{pp}^{A}(t)$ at $T = 0.5$. The latter are defined as $\Phi_{pp}^{\alpha}(t) = \langle \mathbf{X}_p^{\alpha}(t) \cdot \mathbf{X}_p^{\alpha}(0) \rangle / \langle [X_p^{\alpha}(0)]^2 \rangle$, where the Rouse normal modes [32, 33] of index $p = 0, 1, \ldots N-1$ are given by $\mathbf{X}_p(t) = N^{-1} \sum_{j=1}^{N} \mathbf{r}_j(t) \cos[jp\pi/N]$. Figure 6(a) displays, at $T = 0.45$, angular correlators $C_n^{(b)A}(t)$ for the bond vector, $\mathbf{b}(t)$, between consecutive monomers. Such correlators are defined as $C_n^{(b)A}(t) = P_n[\cos\theta(t)]$, where P_n is the Legendre polynomial of order n, and $\cos\theta(t) = \langle \mathbf{b}(t) \cdot \mathbf{b}(0) \rangle / \langle b^2(0) \rangle$. Angular correlators $C_n^{(e)A}(t)$ for the chain end-to-end vector, $\mathbf{e}(t)$, are defined in an analogous way, with $\cos\theta(t) = \langle \mathbf{e}(t) \cdot \mathbf{e}(0) \rangle / \langle e^2(0) \rangle$. Data for $C_n^{(e)A}(t)$ at $T = 0.5$ are given in figure 6(b).

Lines in figures 4–6 are fits of the α-decay of the mentioned correlators to a power-law series expansion like equation (1) with a common von Schweidler exponent $b = 0.30$. Only terms up to second order (t^{2b}) are included in the fit procedure (in the following, references to this equation will be understood as being limited to second order). It must be stressed that the validity of equation (1) for the early-middle α-decay must not be assessed by the length of the

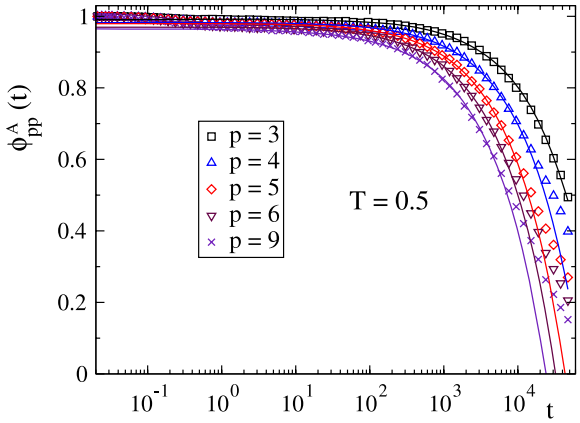

Figure 5. Symbols: for different values of p, correlators of the Rouse pth modes, $\phi^{A}_{pp}(t)$, of the A-chains. Lines are fits to equation (1) with an exponent $b = 0.30$. The temperature is $T = 0.5$.

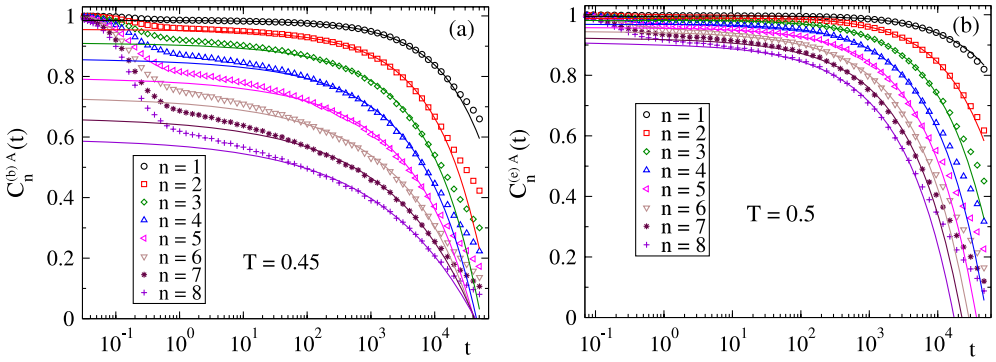

Figure 6. (a) Symbols correspond, for different values of n, to angular correlators $C_n^{(b)A}(t)$ of the bond vector of the A-chains. Lines are fits to equation (1) with an exponent $b = 0.30$. The temperature is $T = 0.45$. (b) As (a) for angular correlators $C_n^{(e)A}(t)$ of the end-to-end vector. The temperature is $T = 0.5$.

vertical interval of $\Phi(t)$ that it is able to cover. Indeed, if the relaxation time of the analysed correlator is much longer than the α-time τ_α, the vertical interval described by (1) will be rather small, as we will discuss below. The prefactors h_Φ and $h_\Phi^{(2)}$ in (1), which yield the amplitude of the decay, are generally in anti-phase with Φ^c [34, 36, 38, 42] and are small for large values of the latter. Hence, for correlators with high plateaux, equation (1) will only describe a small *vertical* interval of the decay. On the contrary, validity of (1) is given by the extension of the time window (i.e. *horizontal* interval) that it is able to describe. In the present case a good description of the simulation data is obtained over three time decades for the lowest investigated temperature, a time window of validity which is typically achieved in simulations. It must be noted that such a time window corresponds to a specific dynamic regime, the early-middle stage of the structural α-relaxation. However, relaxation of a given correlator to a small value (e.g. $x = 0.2$) can occur at a very different timescale τ_x^Φ. This is the case of, for example, low-index correlators of Rouse modes or chain end-to-end vectors. The latter show a decay much slower than density–density correlators $F_{AA}(q, t)$ at the maximum of $S_{AA}(q)$ ($q = 4.5$), which properly probe the timescale τ_α of the structural α-relaxation for the A-chains. For $F_{AA}(q, t)$

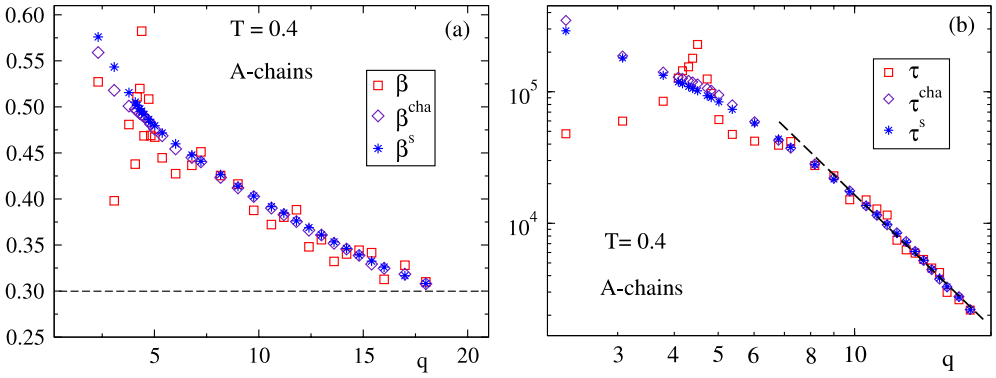

Figure 7. (a) The q-dependence of the stretching exponent of different correlators for the A-monomers (see text for notations) at temperature $T = 0.4$. The dashed line indicates the large-q limit $\beta(q) = b = 0.30$. (b) As (a) for the corresponding KWW times (see text). The dashed line corresponds to the power law $\propto q^{-1/b}$, with $b = 0.30$.

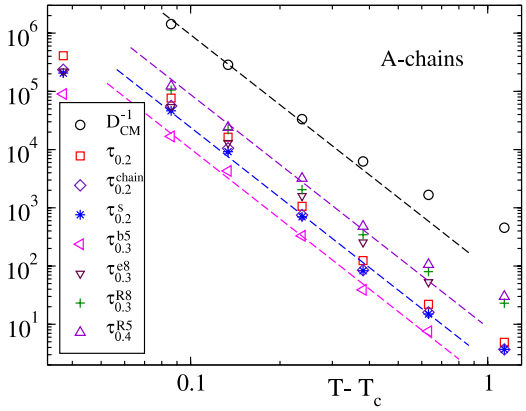

Figure 8. Symbols: inverse diffusivity (circles) and relaxation times of different correlators for the A-monomers (see text for notation). The wavevector for $\tau_{0.2}$, $\tau^{\rm chain}_{0.2}$, and $\tau^{\rm s}_{0.2}$ is $q = 4.6$. The dashed lines are (from top to bottom) fits of $D^{-1}_{\rm CM}$, $\tau^{\rm R5}_{0.4}$, $\tau^{\rm s}_{0.2}$, and $\tau^{\rm b5}_{0.3}$ to the MCT power law $\propto (T - T_{\rm c})^{-\gamma}$, with $T_{\rm c} = 0.37$ and $\gamma = 4.0$.

we find $\tau_{0.2} = 1.7 \times 10^4$ at $T = 0.5$, while relaxation times at the same temperature for low indexes of $\Phi^{\rm A}_{pp}(t)$ and $C^{({\rm e})\rm A}_n(t)$ are clearly much longer (see figures 5 and 6(b)). Having said this, MCT establishes that asymptotic expansions such as (1) will be observed for any dynamic correlator in the specific early-middle time window of the α-relaxation, the process investigated here.

Figure 7 shows a test of the MCT predictions $\beta(q \to \infty) = b$ and $\tau(q \to \infty) \propto q^{-1/b}$. The stretching exponents β, $\beta^{\rm cha}$, and $\beta^{\rm s}$, correspond, respectively, to the density–density, intrachain coherent and self-correlators of the A-monomers at $T = 0.4$, and are obtained as fits of the decay from the plateau to a KWW function. The corresponding KWW times are respectively denoted as τ, $\tau^{\rm cha}$, and $\tau^{\rm s}$. The mentioned large-q predictions for stretching exponents and KWW times are fulfilled with $b = 0.30$, i.e. with the same value of the von Schweidler exponent used in the fits of the dynamic correlators presented in figures 4–6.

The exponent $b = 0.30$ provides, through equations (3) and (4), the values $\lambda = 0.90$, $a = 0.21$, and $\gamma = 4.0$. Now we test the validity of equation (2) with this latter value of

γ. Figure 8 shows the temperature dependence of the relaxation times τ_x^{Φ} of several dynamic correlators Φ for the A-monomers. As mentioned above, these times are defined as those where the corresponding correlator decays to a value x. Notations $\tau_{0.2}$, $\tau_{0.2}^{\text{chain}}$, $\tau_{0.2}^{\text{s}}$, $\tau_{0.3}^{\text{b5}}$, $\tau_{0.3}^{\text{e8}}$, $\tau_{0.3}^{\text{R8}}$, and $\tau_{0.4}^{\text{R5}}$ correspond, respectively, to the correlators $F_{\text{AA}}(q,t)$, $F_{\text{AA}}^{\text{chain}}(q,t)$, $F_{\text{A}}^{\text{s}}(q,t)$, $C_5^{(\text{b})\text{A}}(t)$, $C_8^{(\text{e})\text{A}}(t)$, $\phi_{88}^{\text{A}}(t)$, and $\phi_{55}^{\text{A}}(t)$. The wavevector for the first three correlators is $q = 4.6$, an intermediate value between the main maxima of $S_{\text{AA}}(q)$ and $S_{\text{AA}}^{\text{chain}}(q)$ (see figure 1). The selected values of x are well below the plateau height of the correlator (see figures 4–6). Also displayed is the inverse diffusivity, D_{CM}^{-1}, of the center-of-mass of the A-chains, which is defined as the long-time limit of the ratio $6t/\langle[\Delta r_{\text{A}}^{\text{CM}}(t)]^2\rangle$, where $\langle[\Delta r_{\text{A}}^{\text{CM}}(t)]^2\rangle$ is the corresponding mean squared displacement.

Dashed lines in figure 8 represent fits to the power law (2) by forcing a common critical temperature T_{c} for all the data sets, with a fixed exponent $\gamma = 4.0$, i.e. the value independently determined from the analysis previously presented in figures 4–7. A value $T_{\text{c}} = 0.37$ provides the best global fit with the mentioned constraint. Interestingly, this value is much lower than the one obtained for the homopolymer state [14] at the same investigated packing fraction $\phi = 0.53$, $T_{\text{c}} = 0.52$. The latter value is obviously identical for the limits $x_{\text{B}} = 0$ and 1, since the energy scale ϵ of the model is the same for all the pair interactions, which only differ by the length scale $\sigma_{\alpha\beta}$ (see section 2). Hence, blending at a fixed packing fraction stabilizes the ergodic phase as compared to the homopolymer state, in analogy with the behaviour observed for colloidal binary mixtures of similar size disparity [42–44].

A good description of all the data sets is obtained over more than two decades of relaxation time and inverse diffusivity. As expected, due to the asymptotic character of equation (2), deviations from power-law behaviour occur at high temperature. Such deviations are also present below some ill-defined temperature very close to T_{c}. This feature is often observed if one investigates dynamics at sufficiently low temperatures [45–47] and is usually related with the presence of activated hopping events, which are not accounted for within the ideal version of the MCT.

The analysis of simulation data of the slow A-component that has been presented in figures 4–8 consists of a series of independent tests of several predictions of MCT with a common set of values of the critical exponents. Therefore it provides a robust determination of such values, and in particular of the exponent parameter $\lambda = 0.90$ from which the rest of the exponents are derived through equations (3) and (4). This value of λ is unusually large, as compared to those typical of one-component systems, as monodisperse hard spheres [36] ($\lambda = 0.74$), simplified models of *ortho*-terphenyl [39] ($\lambda = 0.76$), silica [48] ($\lambda = 0.71$), water [49] ($\lambda = 0.78$), or bead–spring homopolymers [50] ($\lambda = 0.72$). In the following subsection we discuss the consequences of the large value of λ obtained here.

6. Dynamics of the fast component in the blend

Now we analyse the dynamics of the fast B-component. Figure 9(a) shows simulation results for the intrachain coherent correlator, $F_{\text{BB}}^{\text{chain}}(q,t)$, at temperature $T = 0.4$. As previously reported in [14] for the total density–density correlator $F_{\text{BB}}(q,t)$, a concave-to-convex crossover is observed by varying the wavevector. For intermediate values of the latter, a purely logarithmic decay occurs over more than three time decades. Following a procedure analogous to that of [14], we have analysed the decay of $F_{\text{BB}}^{\text{chain}}(q,t)$ in terms of a logarithmic expansion,

$$F_{\text{BB}}^{\text{chain}}(q,t) = f_q^{\text{c}} - H_q \ln(t/\tau_\sigma) + H_q^{(2)} \ln^2(t/\tau_\sigma) + \text{O}[\ln^3(t/\tau_\sigma)], \tag{5}$$

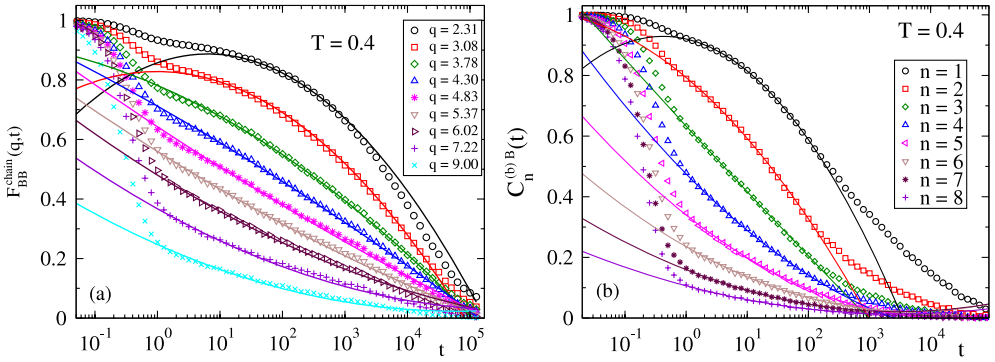

Figure 9. (a) Symbols correspond, for different wavevectors, to intrachain coherent correlators for B–B pairs, $F_{\mathrm{BB}}^{\mathrm{chain}}(q,t)$, at $T = 0.4$. Lines are fits to the logarithmic expansion (5). (b) As (a) for the angular correlators $C_n^{(\mathrm{b})\mathrm{B}}(t)$ of the bond vector of the B-chains.

with $\tau_\sigma \sim t_\sigma$, instead of the von Schweidler series (1) used for the A-monomers (we will discuss this point below). Within the framework of MCT, logarithmic expansions of dynamic correlators are associated with the presence of a nearby higher-order transition [17–19]. The latter is characterized by a value of the exponent parameter $\lambda = 1$, though analogous predictions are expected for sufficiently large values $\lambda \to 1^-$ as the one obtained here, $\lambda = 0.90$ (see section 5). Equation (5) provides a good description of the decay of correlators displayed in figure 9(a). Analogous fits are shown in figure 9(b) for the orientational correlators $C_n^{(\mathrm{b})\mathrm{B}}(t)$ of the bond vector, evaluated for different values of n. In this case the validity of the logarithmic expansion is observed, at the same temperature, over a shorter time interval. Figure 10 shows the values of the coefficients f_q^{c}, H_q, and $H_q^{(2)}$ obtained from the corresponding fits of $F_{\mathrm{BB}}^{\mathrm{chain}}(q,t)$ at two different temperatures ($T = 0.4$ and 0.5). The term f_q^{c} is the critical non-ergodicity parameter, which is associated with the transition point. Therefore its values at different wavevectors must not depend on the state point at which they are obtained as fit parameters. This is confirmed by the numerical values displayed in figure 10(a). According to MCT, the prefactor H_q is factorized as the product of two terms. One of them only depends on the state point and the other one on the wavevector [19]. Therefore the values of H_q evaluated at different state points must obey scaling behaviour. This feature is also confirmed by data in figure 10(b). Also in agreement with MCT expectations [19], the obtained values of the second prefactor $H_q^{(2)}$ are smaller than H_q and incompatible with scaling behaviour (see figure 10(c)).

Results presented in figures 9 and 10 support the similar analysis performed in [14] for density–density correlations of the B-monomers, $F_{\mathrm{BB}}(q,t)$. It must be stressed that the choice of equation (5) for describing relaxation of correlators for B-monomers is not, in principle, in contradiction with the description of the same correlators for the A-monomers in terms of the power-law series (1). Both equations are *series expansions* whose convergence depends on the analysed region of the control parameter space. For the case of higher-order transitions ($\lambda = 1$), or more generally for transitions with $\lambda \to 1^-$, there are q-dependent paths in the control parameter space where the series (5) is rapidly convergent. In particular, for each wavevector there are optimal paths where $H_q^{(2)} = 0$. Along these paths the corresponding correlator will exhibit a purely logarithmic decay [19]. Moreover, by properly tuning the control parameters or the wavevector, it is possible to change the sign of $H_q^{(2)}$ and, as a consequence, inducing a concave-to-convex crossover in the shape of the decay [19], as observed in figure 9. Since from the analysis of dynamic correlators for the A-monomers we have determined a value $\lambda = 0.90$,

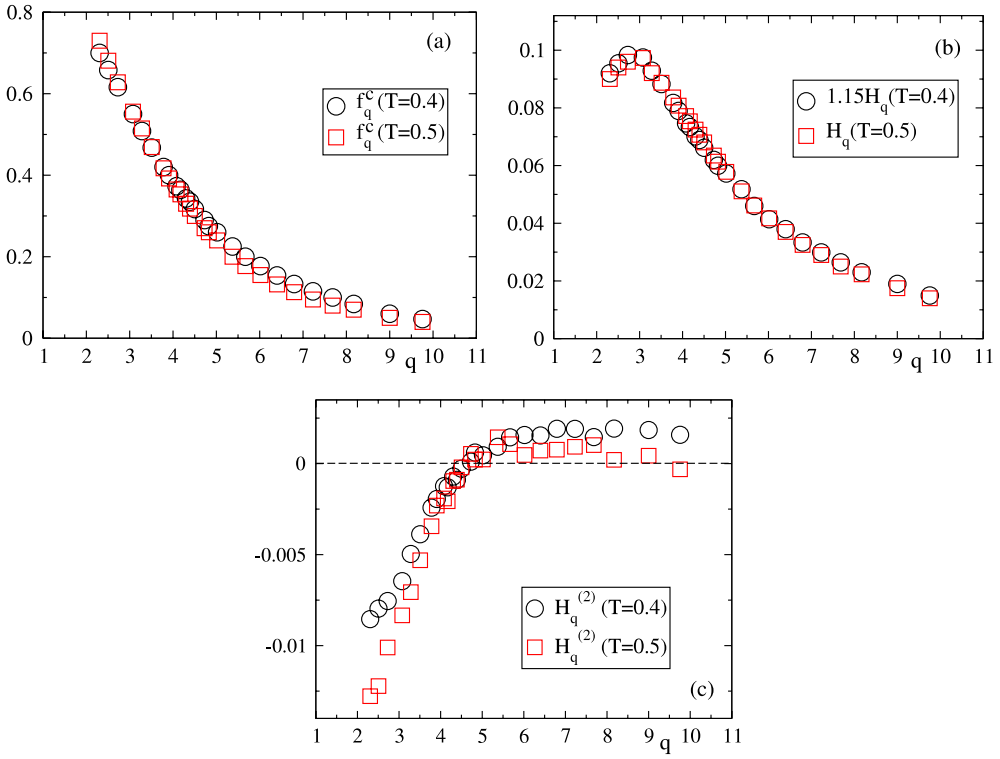

Figure 10. Symbols in (a), (b), and (c) correspond, respectively, to the values of the critical non-ergodicity parameter, f_q^c, and the prefactors H_q and $H_q^{(2)}$ in equation (5), for the intrachain coherent correlator for B–B pairs, $F_{BB}^{chain}(q,t)$. Temperatures are $T = 0.4$ (circles) and $T = 0.5$ (squares).

it might be expected that such correlators will exhibit such features at some state point. Indeed, they are observed at higher temperatures, as shown in figure 11 for $F_{AA}^{chain}(q,t)$ at $T = 1.0$. The decay exhibits a clear concave-to-convex crossover by tuning the wavevector. Logarithmic relaxation covers two time decades for $q \approx 5.2$.

The fact that features associated with nearby higher-order MCT transitions are observed for the A- and the B-components at very different temperatures must be commented on. As mentioned above, the optimal paths in the control parameter space for the observation of logarithmic relaxation are different for each correlator [19]. The location of these paths is controlled by static correlations [19], which in the present case are very different for the A- and the B-monomers (see figure 1). This difference might explain why anomalous relaxation for both types of monomer is observed at very different temperatures. Unless one moves close to the optimal path in the control parameter space—which usually involves a simultaneous variation of *several* control parameters [17, 19]—logarithmic relaxation vanishes by decreasing temperature, and a standard two-step decay is recovered (see [21] for an illustrative example). This seems to be the case of correlators for the A-monomers, which at low temperature are well described by the von Schweidler power-law series (1). A similar result has also been observed for mixtures of large and small non-bonded particles [23]. Still, a satisfactory answer to this point can only be obtained by solving the MCT equations for this system.

Figure 12 displays, for the B-chains at $T = 0.4$, results for the density self-correlators, $F_B^s(q,t)$. A reliable fit (over more than one time decade) of the corresponding decays to

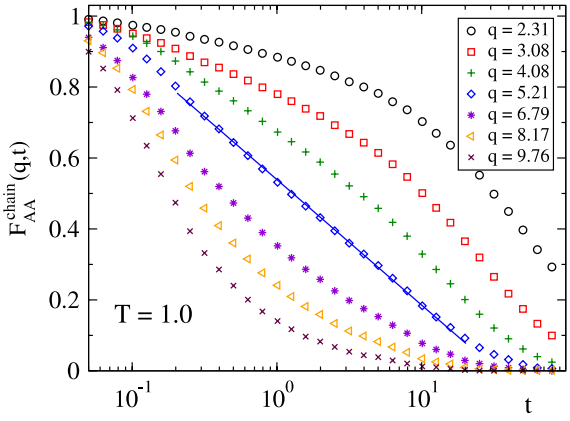

Figure 11. Symbols: for different wavevectors, intrachain coherent correlator for A–A pairs, $F_{AA}^{chain}(q,t)$, at $T = 1.0$. The straight line indicates logarithmic behaviour over two time decades.

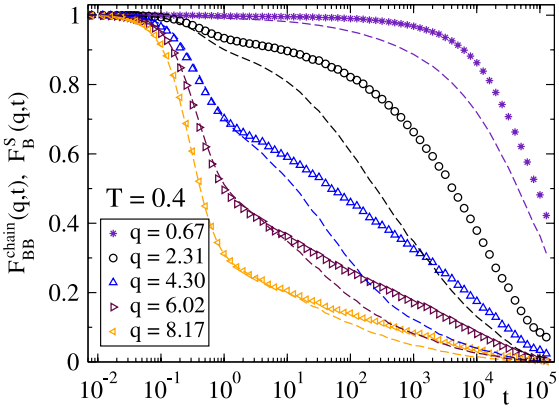

Figure 12. Comparison, at $T = 0.4$, between the intrachain coherent ($F_{BB}^{chain}(q,t)$, symbols) and self-correlators ($F_{B}^{s}(q,t)$, dashed lines) for the B-monomers. The wavevectors for the latter are, from top to bottom, the same ones as for the former (see legend).

equation (1)—with any common exponent b for all wavevectors—or (5) was not possible. Similar tests were also unsuccessful for correlators probing reorientations of chain end-to-end vectors, $C_n^{(e)B}(t)$, and relaxation of Rouse modes, $\Phi_{pp}^{B}(t)$, of the B-chains. The reason for the apparent failure for the B-chains, or at least the limited range of validity, of the former equations for these correlators remains to be understood. It might be that this feature is connected to a non-universal character of the asymptotic expansions (1), (5) for binary mixtures with very different timescales for their respective density fluctuations, and that despite this non-universality, MCT can still reproduce the behaviour of the mentioned correlators for the B-chains. It might also be related to the presence of hopping events intervening in self-motions of the B-monomers (see below). As we argue in the following, there are results in the literature that support these possibilities.

Numerical solutions of the MCT equations have recently been presented for sodium silicate melts and compared with simulation results [51]. In these systems the fast sodium atoms and the slow silica matrix exhibit a strong timescale separation similar to that observed here for the A- and B-chains [51, 52]. Though an analysis of density–density correlators for the different

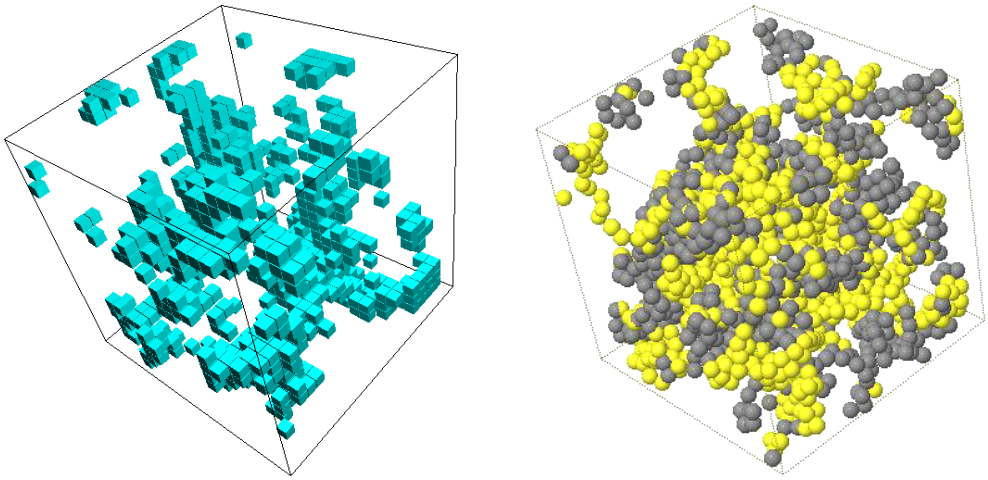

Figure 13. Left side: cubic boxes represent the $N_B N$ subcells (of size $\approx\sigma_{BB}^3$) in the simulation box which have been visited more times by the B-monomers during a simulation time of $t = 5 \times 10^4$, for $T = 0.5$. Right side: initial (dark spheres) and final (light spheres) configuration of the B-monomers for the latter simulation interval. The same orientation of the simulation cell is used in both figures.

atomic species, as well as of self-correlators for silicon and oxygen, have provided a consistent test of MCT predictions with a common set of dynamic exponents [52], self-correlators $F^s(q,t)$ of the sodium atoms do not show [52], as in the present case, a reliable time interval for apparent validity of equations (1) or (5). Still, the corresponding numerical solutions of MCT equations reported in [51] do reproduce the qualitative behaviour of $F^s(q,t)$ for the sodium atoms. In particular, MCT accounts for the unusual timescale separation between self- and collective-density correlators which is observed for the sodium atoms. This feature is assigned [52–56] to preferential diffusion along a long-living structure of channels induced by the much slower relaxation of the silica matrix, which leads, for the alkali ions, to a fast decay of self-correlations as compared to collective correlations.

Figure 12 shows a comparison between self-correlators and intrachain coherent correlators for the B-chains at $T = 0.4$. Both correlators only converge to each other in the limit of large-q. Since, due to the low concentration of the B-component, intrachain coherent correlators for the B-chains exhibit only small differences (not shown) with density–density correlators for *all* the B–B pairs, the large timescale separation between $F_B^s(q,t)$ and $F_{BB}^{cha}(q,t)$ presented in figure 12 is a feature analogous to that noted above for alkali ions in silica matrices [52]. Indeed, following a procedure similar to that presented in [53] for the sodium atoms, we have determined a similar structure of channels for preferential motion of the B-chains. We have divided the simulation box in cubic subcells of size $\approx\sigma_{BB}^3$ and computed, for a trajectory of the system, the number of times each subcell is visited by a B-monomer. Figure 13 displays, at $T = 0.5$, the $N_B N$ (a number equal to that of B-monomers) most visited subcells for a simulation time $t = 5 \times 10^4$. The latter is much longer than the time for structural relaxation of the B-monomers at that temperature. As shown in figure 13, the mentioned subcells are not randomly distributed but form connected clusters, in analogy with results reported in [53] for sodium in silica matrices.

In figure 13 we also display the initial and final configuration of the B-monomers for the mentioned simulation interval $t = 5 \times 10^4$ used for the computation of the most visited subcells.

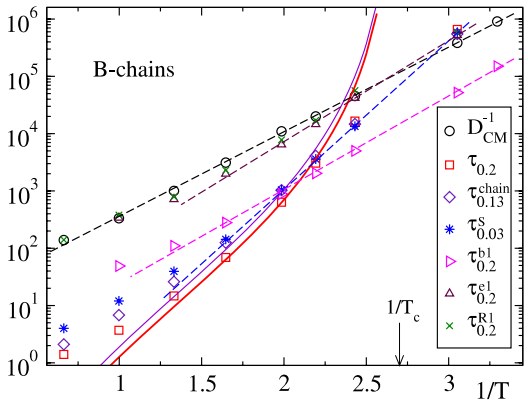

Figure 14. Symbols: inverse diffusivity (circles) and relaxation times of different correlators for the B-monomers (see text for notation). The wavevector for $\tau_{0.2}$, $\tau_{0.13}^{\rm chain}$, and $\tau_{0.03}^{\rm s}$ is $q = 4.6$. The thick and thin solid lines are fits of, respectively, $\tau_{0.2}$ and $\tau_{0.13}^{\rm chain}$ to a MCT power law $\propto (T - T_{\rm c})^{-\gamma}$, with $T_{\rm c} = 0.37$ and $\gamma = 4.0$. The arrow indicates the inverse value of $T_{\rm c}$. The dashed lines are (from top to bottom) fits of $D_{\rm CM}^{-1}$, $\tau_{0.2}^{\rm e1}$, $\tau_{0.2}^{\rm b1}$, and $\tau_{0.03}^{\rm s}$ to Arrhenius behaviour, $\propto \exp(E/T)$. The activation energies are, respectively, $E = 3.4$, 4.1, 3.8, and 5.9.

As expected (t is much longer than the structural relaxation time for B-monomers) both configurations are fully decorrelated. Therefore the mentioned channel structure is not a trivial consequence of the *static* correlations for the B–B pairs, which also form a cluster structure (figure 2). It is instead induced by the timescale separation of the *dynamic* correlations, which are much slower for the confining matrix formed by the A-chains. The channel structure will only vanish when any region of the simulation cell can be visited by the B-monomers with the same probability. This can only occur at much longer times probing full structural relaxation of the A-component. A detailed static and dynamic characterization of this channel structure is beyond the scope of this paper and will be presented elsewhere.

Finally, it must be mentioned that the observed decoupling between intrachain collective and self-correlators is exhibited only by the B-chains in the blend. For the A-chains in the blend, as well as for the homopolymers, we have observed only small differences for the latter correlators. Decoupling between self- and collective intrachain dynamics is indeed a rather unusual feature, at odds with expectations from the standard Rouse model [32, 33]. This observation in the simple bead–spring blend investigated here is supported by recent neutron scattering experiments on PEO/PMMA at a low PEO concentration [57]. Whether numerical solutions of MCT equations are also able, in analogy with the case of alkali ions in silica, to give account for this feature is an open question.

Figure 14 shows the temperature dependence of the relaxation times for several dynamic correlators probing relaxation of the B-component. Notations $\tau_{0.2}$, $\tau_{0.13}^{\rm chain}$, $\tau_{0.03}^{\rm s}$, $\tau_{0.2}^{\rm b1}$, $\tau_{0.2}^{\rm e1}$, and $\tau_{0.2}^{\rm R1}$ correspond, respectively, to the correlators $F_{\rm BB}(q,t)$, $F_{\rm BB}^{\rm chain}(q,t)$, $F_{\rm B}^{\rm s}(q,t)$, $C_1^{\rm (b)B}(t)$, $C_1^{\rm (e)B}(t)$, and $\phi_{11}^{\rm B}(t)$. The wavevector for the first three correlators is $q = 4.6$. Also included is the inverse diffusivity of the center-of-mass for the B-chains. The set of data shown in figure 14 exhibits a behaviour rather different from similar quantities for the A-chains displayed in figure 8. Only relaxation times for collective density correlations, $F_{\rm BB}(q,t)$ and $F_{\rm BB}^{\rm chain}(q,t)$, show qualitative agreement with the MCT power law $\propto (T - 0.37)^{-4.0}$ derived from data of the A-monomers. As expected, deviations occur at temperatures very close to $T_{\rm c}$. The rest of the quantities displayed in figure 14 are incompatible with power-law behaviour. They show instead an apparent Arrhenius dependence, $\propto \exp(E/T)$, from

moderate to the lowest investigated temperatures. This feature is demonstrated in figure 14 by the linear behaviour observed by representing data on a logarithmic scale versus (linear) $1/T$. The obtained activation energies E vary between 3.4 for the center-of-mass diffusivity and 5.9 for the relaxation time of density self-correlations. The observed Arrhenius behaviour suggests that strong hopping events intervene in the structural relaxation of the B-chains, similar to observations for alkaline ions in silica [58]. These events seem to affect more strongly the self- than the collective density correlations, for which a power-law behaviour can be observed over two decades in relaxation time for temperatures above T_c. It remains to be understood whether such hopping events—which are not included in the ideal version of MCT—are related to the mentioned reduction of the range of validity of equations (1) or (5) for the corresponding correlators. It is worth mentioning that the latter possibility might be the case for sodium atoms in silica. Numerical solutions of the MCT equations reported in [51], though reproducing the observed qualitative behaviour, underestimate the strength of the decay exhibited in simulations for self-correlators $F^s(q,t)$ of sodium. Hence, the presence of hopping events presumably accelerates relaxation as compared to theoretical predictions.

Finally, it is worth remarking that the observed Arrhenius-like temperature dependence for $\tau^{b1}_{0.2}$ and $\tau^{s}_{0.03}$ is consistent with experimental observations, for the fast component, in real polymer blends with large dynamic asymmetry by, respectively, dielectric spectroscopy [7, 8, 10] and neutron scattering [13], which probe relaxation times of similar dynamic correlators. Arrhenius behaviour for self-dynamics is also observed for the case of alkali ions in silica [58] or for water reorientation in polymer matrices [59]. This common Arrhenius-like behaviour in very different systems suggests a universal feature for low concentrations of fast molecules in slow host media with interconnected voids.

7. Conclusions

We have presented a computational investigation on the structural relaxation of a simple bead–spring model for polymer blends with large dynamic asymmetry. We have computed a large set of dynamic correlators probing relaxation of density fluctuations, Rouse modes, and reorientation of bond and chain end-to-end vectors. Results have been discussed within the framework of the mode coupling theory (MCT) for the glass transition. A robust test of MCT predictions has been achieved through a description of the different analysed correlators with a common set of dynamic exponents, though for some correlators probing dynamics of the fast component MCT asymptotic laws are apparently not observed. The observation of Arrhenius-like behaviour suggests that this breakdown might be associated with strong hopping events intervening in relaxation of the fast component.

An unusually large value of the exponent parameter λ has been obtained, close to the upper limit ($\lambda = 1$) characteristic of higher-order MCT transitions. According to MCT predictions, the anomalous relaxation features observed in the present system, as logarithmic decays or concave-to-convex crossovers in density correlators, might be associated with that underlying higher-order scenario. An investigation of the case of extreme dilution, where each individual chain of the fast component is surrounded only by chains of the slow component (and where an asymptotic dynamic limit is expected [6]), would be computationally expensive. Still, we expect that a qualitatively similar scenario of anomalous relaxation will be observed. Since chain connectivity will always guarantee the presence of neighbouring monomers of the same species for a given monomer of the fast component, coexistence of bulk-like caging and confinement for the fast component would be present even at extreme dilution, inducing the higher-order scenario. On the other hand, a progressive increase in the concentration of the fast component will reduce the timescale separation (i.e. the dynamic asymmetry) between the

two components, and confinement effects will finally vanish. In that situation the standard MCT relaxation scenario (as observed for the homopolymer case) will be recovered. The large collection of results presented here might motivate theoretical work on structural relaxation in polymer blends with large dynamic asymmetry, and in particular, numerical solutions of the MCT equations to confirm the suggested higher-order scenario.

Acknowledgments

We acknowledge financial support from the projects NMP3-CT-2004-502235 (SoftComp), MAT2004-01017 (Spain), and 206.215-13568/2001 (GV-UPV/EHU Spain). AJM acknowledges support from DIPC (Spain).

References

[1] Kant R, Kumar S K and Colby R H 2003 *Macromolecules* **36** 10087
[2] Lodge T P and McLeish T C B 2000 *Macromolecules* **33** 5278
[3] Kumar S K, Shenogin S and Colby R 2007 *Macromolecules* **40** 5759
[4] Cangialosi D, Schwartz G A, Alegría A and Colmenero J 2005 *J. Chem. Phys.* **123** 144908
Schwartz G A, Cangialosi D, Alegría A and Colmenero J 2006 *J. Chem. Phys.* **124** 154904
[5] Lartigue C, Guillermo A and Cohen-Addad J P 1997 *J. Polym. Sci.* B **35** 1095
[6] Lutz T R, He Y Y, Ediger M D, Cao H H, Lin G X and Jones A A 2003 *Macromolecules* **36** 1724
[7] Lorthioir C, Alegría A and Colmenero J 2003 *Phys. Rev.* E **68** 031805
[8] Sy J W and Mijovic J 2000 *Macromolecules* **33** 933
[9] Roland C M, McGrath K J and Casalini R 2006 *Macromolecules* **39** 3581
[10] Schwartz G A, Colmenero J and Alegría A 2007 *Macromolecules* **40** 3246
[11] Taneko H, Kobayashi M and Aikawa T 2006 *Macromolecules* **39** 2183
[12] Genix A C, Arbe A, Alvarez F, Colmenero J, Willner L and Richter D 2005 *Phys. Rev.* E **72** 031808
[13] Tyagi M, Arbe A, Colmenero J, Frick B and Stewart J R 2006 *Macromolecules* **39** 3007
[14] Moreno A J and Colmenero J 2006 *J. Chem. Phys.* **124** 184906
[15] Götze W 1991 *Liquids, Freezing and Glass Transition* (*Les Houches 1989*) ed J P Hansen, D Levesque and J Zinn-Justin (Amsterdam: North-Holland) p 287
[16] Götze W and Sjögren L 1992 *Rep. Prog. Phys.* **55** 241
[17] Götze W and Haussmann R 1988 *Z. Phys.* B **72** 403
Götze W and Sperl M 2002 *Phys. Rev.* E **66** 011405
[18] Dawson K, Foffi G, Fuchs M, Götze W, Sciortino F, Sperl M, Tartaglia P, Voigtmann T and Zaccarelli E 2000 *Phys. Rev.* E **63** 011401
[19] Sperl M 2003 *Phys. Rev.* E **68** 031405
[20] Sciortino F, Tartaglia P and Zaccarelli E 2003 *Phys. Rev. Lett.* **91** 268301
[21] Zaccarelli E, Foffi G, Dawson K A, Buldyrev S V, Sciortino F and Tartaglia P 2002 *Phys. Rev.* E **66** 041402
[22] Moreno A J and Colmenero J 2006 *Phys. Rev.* E **74** 021409
[23] Moreno A J and Colmenero J 2006 *J. Chem. Phys.* **125** 164507
[24] Mayer C 2007 *PhD Thesis* Universität Düsseldorf
[25] Bingemann D, Wirth N, Gmeiner J and Rössler E A 2007 *Macromolecules* **40** 5379
[26] Krakoviack V 2007 *Phys. Rev.* E **75** 031503
[27] Grest G S and Kremer K 1986 *Phys. Rev.* A **33** R3628
[28] Kob W and Andersen H C 1995 *Phys. Rev.* E **51** 4626
Kob W and Andersen H C 1995 *Phys. Rev.* E **52** 4134
[29] Bennemann C, Paul W, Binder K and Dunweg B 1998 *Phys. Rev.* E **57** 843
Bennemann C, Baschnagel J and Paul P 1999 *Eur. Phys. J.* B **10** 323
[30] Frenkel D and Smit B 1996 *Understanding Molecular Simulation* (San Diego, CA: Academic)
[31] Aichele M and Baschnagel J 2001 *Eur. Phys. J.* E **5** 229
Aichele M and Baschnagel J 2001 *Eur. Phys. J.* E **5** 245
[32] Teraoka I 2002 *Polymer Solutions* (New York: Wiley)
[33] Doi M and Edwards S F 1986 *The Theory of Polymer Dynamics* (Oxford: Oxford University Press)
[34] Götze W 1999 *J. Phys.: Condens. Matter* **11** A1

[35] Das S P 2004 *Rev. Mod. Phys.* **76** 785
[36] Franosch T, Fuchs M, Götze W, Mayr M R and Singh A P 1997 *Phys. Rev.* E **55** 7153
[37] Fuchs M 1994 *J. Non-Cryst. Solids* **172** 241
[38] Fuchs M, Hofacker I and Latz A 1992 *Phys. Rev.* A **45** 898
[39] Mossa S, Di Leonardo R, Ruocco G and Sampoli M 2000 *Phys. Rev.* E **62** 612
[40] Puertas A M, Fuchs M and Cates M E 2003 *Phys. Rev.* E **67** 031406
[41] Colmenero J, Narros A, Alvarez F, Arbe A and Moreno A J 2007 *J. Phys.: Condens. Matter* **19** 205127
[42] Götze W and Voigtmann T 2003 *Phys. Rev.* E **67** 021502
[43] Williams S R and van Megen W 2001 *Phys. Rev.* E **64** 041502
[44] Foffi G, Götze W, Sciortino F, Tartaglia P and Voigtmann T 2003 *Phys. Rev. Lett.* **91** 085701
[45] Ashwin S S and Sastry S 2003 *J. Phys.: Condens. Matter* **15** S1253
[46] Gallo P, Pellarin R and Rovere M 2003 *Phys. Rev.* E **67** 041202
[47] Flenner E and Szamel G 2005 *Phys. Rev.* E **72** 011205
[48] Horbach J and Kob W 1999 *Phys. Rev.* B **60** 3169
Horbach J and Kob W 2001 *Phys. Rev.* E **64** 041503
[49] Sciortino F, Fabbian L, Chen S H and Tartaglia P 1997 *Phys. Rev.* E **56** 5397
[50] Baschnagel J and Varnik F 2005 *J. Phys.: Condens. Matter* **17** R851
[51] Voigtmann T and Horbach J 2006 *Europhys. Lett.* **74** 459
[52] Horbach J and Kob W 2002 *J. Phys.: Condens. Matter* **14** 9237
Horbach J, Kob W and Binder K 2002 *Phys. Rev. Lett.* **88** 125502
[53] Jund P, Kob W and Jullien R 2001 *Phys. Rev.* B **64** 134303
[54] Greaves G N 1985 *J. Non-Cryst. Solids* **71** 203
[55] Lammert H, Kunow M and Heuer A 2003 *Phys. Rev. Lett.* **90** 215901
[56] Meyer A, Horbach J, Kob W, Kargl F and Schober H 2004 *Phys. Rev. Lett.* **93** 027801
Kargl F, Meyer A, Koza M M and Schober H 2006 *Phys. Rev.* B **74** 014304
[57] Niedzwiedz K, Wischnewski A, Monkenbusch M, Richter D, Genix A C, Arbe A, Colmenero J, Strauch M and Straube E 2007 *Phys. Rev. Lett.* **98** 168301
[58] Horbach J, Kob W and Binder K 2001 *Chem. Geol.* **174** 87
[59] Cerveny S, Schwartz G A, Bergman R and Swenson J 2004 *Phys. Rev. Lett.* **93** 245702
Cerveny S, Schwartz G A, Alegría A, Bergman R and Swenson J 2006 *J. Chem. Phys.* **124** 194501